

Markov-chain reconstruction of the 2dF Galaxy Redshift Survey real-space power spectrum

Will J. Percival

Institute for Astronomy, University of Edinburgh, Royal Observatory, Blackford Hill, Edinburgh EH9 3HJ, UK

ABSTRACT

The real-space power spectrum of L_* galaxies measured from the 2dF Galaxy Redshift Survey (2dFGRS) is presented. Markov-Chain Monte-Carlo (MCMC) sampling was used to fit radial and angular modes resulting from a Spherical Harmonics decomposition of the 2dFGRS overdensity field (described in Percival et al. 2004) with 16 real-space power spectrum values and linear redshift-space distortion parameter $\beta(L_*, 0)$. The recovered marginalised band-powers are compared to previous estimates of galaxy power spectra. Additionally, we provide a simple model for the 17 dimensional likelihood hyper-surface in order to allow the likelihood to be quickly estimated given a set of model band-powers and $\beta(L_*, 0)$. The likelihood surface is not well approximated by a multi-variate Gaussian distribution with model-independent covariances. Instead, a model is presented in which the distribution of each band-power has a Gaussian distribution in a combination of the band-power and its logarithm. The relative contribution of each component was determined by fitting the MCMC output. Using these distributions, we demonstrate how the likelihood of a given cosmological model can be quickly and accurately estimated, and use a simple set of models to compare estimated likelihoods with likelihoods calculated using the full Spherical Harmonics procedure. All of the data are made publically available (from <http://www.roe.ac.uk/~wjp/>), enabling the Spherical Harmonics decomposition of the 2dFGRS of Percival et al. (2004) to be easily used as a cosmological constraint.

Key words: large-scale structure of Universe, cosmological parameters

1 INTRODUCTION

In addition to a wealth of information about the physics of galaxy formation, galaxy surveys also provide a statistical measure of the large-scale primordial density perturbations. If, as is theoretically expected, the density field on large-scales is well-approximated by a random-phase Gaussian distribution, then the power spectrum provides a statistically complete description of the field. Given a galaxy redshift survey, the most direct route to an approximation to the power spectrum is to decompose the overdensity distribution into Fourier modes (e.g. Feldman, Kaiser & Peacock 1994). However, systematic observed distortions in the radial direction caused by the coherent peculiar velocities of galaxies are difficult to incorporate into a model of a Fourier decomposition.

Consequently, methods to decompose the galaxy overdensity field into 3-dimensional bases consisting of radial and angular functionals have been developed by a number of groups (Heavens & Taylor 1995; Fisher et al. 1994;1995; Hamilton, Tegmark & Padmanabhan 2000). By splitting the basis into radial and angular components, radial redshift-space distortions can be readily included in the analysis method. Recently, the 2dFGRS and SDSS galaxy redshift surveys have both been analysed in this way (Percival et al.

2004;P04, Tegmark et al. 2004) resulting in tight constraints on both the power spectrum shape and the redshift-space distortions. Other analyses of 2-point statistics measured from these surveys include Percival et al. (2001) and Cole et al. (2004) who decomposed the 2dFGRS into Fourier modes and Pope et al. (2004) who undertook a Karhunen-Loève eigenmode analysis of the SDSS based on the correlation function of counts-in-cells.

In this paper we build upon the analysis of P04 who decomposed the 2dFGRS overdensity field into an orthonormal basis of spherical harmonics and spherical Bessel functions. Throughout we refer to such a basis as a Spherical Harmonics basis. In P04, cosmological models were tested against combinations of the radial and angular modes calculated for the decomposed density field. The procedure for calculating the likelihood of each model required inversion of a large covariance matrix ($\sim 1800 \times 1800$) and was computationally expensive. It would obviously be advantageous if the same Likelihood surface could be recovered without having to invert a large matrix for each cosmological model.

The Markov-chain Monte-Carlo (MCMC) technique provides a method for mapping a likelihood surface, providing both marginalised parameters and information about the form of the surface. In this paper, we use the MCMC technique to map the true

likelihood surface as a function of 16 power spectrum band-powers and $\beta(L_*, 0)$. Here $\beta(L_*, 0) \equiv \Omega_m^{0.6}/b(L_*, 0)$ is a measure of the increased fluctuation amplitude for present day L_* galaxies caused by the linear movement of matter onto density peaks and out from voids (Kaiser 1987). Ω_m is the present day matter density and $b(L_*, 0)$ is the present day bias of L_* galaxies. The resulting sampling of the likelihood surface provides an estimate of the real-space galaxy power spectrum through the marginalised power spectrum band-powers (presented in Section 4). In addition, we fit models to the distribution of each band-power, marginalised over the other parameters (Section 6). The distributions are assumed to be Gaussian in a combination of the band-power and its logarithm. Simply assuming a Gaussian distribution in each parameter and model-independent covariances could potentially bias the likelihood estimates. This is directly analogous to the problem of compressing CMB maps into angular band-powers, and the use of those band-powers to estimate the true likelihood surface (e.g. Bond Jaffe & Knox 2000). The model of the likelihood surface can be used to quickly estimate the likelihood of any theoretical power spectrum and $\beta(L_*, 0)$. In Section 7 the likelihood surface estimated for a simple set of cosmological models from these distributions is shown to be in excellent agreement with the original likelihood surface.

2 THE SPHERICAL HARMONICS DECOMPOSITION

This paper builds upon the Spherical Harmonics decomposition of the 2dFGRS overdensity field presented in, and completely described by P04. This description is not replicated here. Instead, we discuss the key points of the P04 analysis which are relevant for the results presented in this paper. This includes a detailed discussion of the likelihood calculation performed in P04 as this provides the benchmark against which we test the accuracy that can be achieved from the compressed data set.

2.1 The methodology of P04

The formalism used by P04 was based in part on that developed by Heavens & Taylor (1995) and described by Tadros et al. (1999). First, the galaxy overdensity field is decomposed into an orthonormal basis consisting of spherical Bessel functions and spherical harmonics. A constant galaxy clustering (CGC) model is assumed, where the amplitude of comoving galaxy clustering is independent of redshift, although it is assumed to be dependent on galaxy luminosity through the relation of Norberg et al. (2001). Each galaxy is weighted using this model so that the measured power spectrum corresponds to that of L_* galaxies (using the method developed in Percival, Verde & Peacock 2004).

To calculate the likelihood of a given cosmological model, the expected covariances between modes have to be calculated. The primary difficulty with this calculation is correctly accounting for the geometry of the 2dFGRS sample, which results in a significant convolution of the true power, and is performed as a discrete sum over Spherical Harmonic modes in a computationally intensive part of the adopted procedure. For computational convenience, and to simplify the real-space shape of the window function, the 2dFGRS sample was split into two wedge shaped components – the NGP and SGP regions of the 2dFGRS (Colless et al. 2003).

In addition to direct corrections for the survey geometry, the effects of redshift-space distortions are also included at this

stage. A first order correction is made for the large-scale redshift-space distortions which are linearly dependent on the density field through $\beta(L_*, 0)$. Because we decompose along radial modes, a far-field approximation (Kaiser 1987) is not required, and the geometry of the distortions is correctly accounted for. A contribution to the observed radial clustering from the small-scale velocity dispersion of galaxies is also included using an additional convolution in the radial direction. The modes chosen cover sufficiently large scales that the exact form of this convolution was unimportant. This convolution provides a statistical model for the fingers-of-god distortions and could be replaced by a more direct method such as the compression of clumps along the line of sight (as favoured by Tegmark et al. 2004).

The transformation between the Spherical Harmonics and the 3D Fourier basis is unitary, so the length of a complex vector is preserved. Consequently, for each Spherical Harmonics basis element we can associate a Fourier k -mode, and a Spherical Harmonics decomposition can be directly related to the standard Fourier power spectrum. The P04 decomposition of the overdensity field resulted in 86667 Spherical Harmonic modes with $0.02 < k < 0.15 h \text{ Mpc}^{-1}$. This range of k was chosen to cover most of the cosmological signal without excessive contamination from small-scale effects (see Percival et al. 2001 for details). It is impractical to directly use all of these modes in a likelihood analysis, and the modes were therefore compressed, leaving 1223 & 1785 combinations of modes for the NGP and SGP respectively. The data compression procedure adopted was designed to remove nearly degenerate modes, which could cause numerical problems followed by Karhunen-Loève data compression to optimally reduce the remaining data. Tests have shown that the inclusion of further modes did not significantly improve the cosmological results from the analysis. The speed of the analysis method depends on the cube of the number of modes: with the current mode number, the analysis of P04 takes approximately 1 month to run on a single top-of-the-line desktop computer, to perform the decomposition and calculate the covariance matrix components. The MCMC analysis of the likelihood surface presented in this paper takes slightly longer. The compressed data and the corresponding covariance matrices are combined to calculate the likelihood of a given model assuming Gaussian statistics as described in the next Section.

2.2 Likelihood calculation

For a Gaussian random field, the decomposition of the 2dFGRS overdensity field obviously follows Gaussian statistics. The likelihood of a cosmological model parameterized by the power spectrum $P(k)$ and linear redshift-space distortion parameter $\beta(L_*, 0)$ is given by

$$\mathcal{L}_{\text{true}}[\mathbf{D}|\beta(L_*, 0), P(k)] = \frac{1}{(2\pi)^{N/2} |\mathbf{C}|^{1/2}} \exp \left[-\frac{1}{2} \mathbf{D}^T \mathbf{C}^{-1} \mathbf{D} \right], \quad (1)$$

where N gives the number of data points to be tested, \mathbf{C} is the covariance matrix, and \mathbf{D} is a linear combination of the Spherical Harmonics modes. Note that the likelihood depends on the cosmological model solely through the covariance matrix \mathbf{C} as $\langle \mathbf{D} \rangle = 0$, independent of cosmology. For computational convenience the covariance matrix was calculated for each model from a series of components covering different ranges in k . Consequently, even for the “true” likelihood as determined in P04, the data are effectively compressed, although 30 intervals in k are used rather than 16.

Because of this, the likelihood comparison presented in Section 7 does not exhaustively test the data compression part of the revised method. The likelihoods for the NGP and SGP regions of the 2dFGRS were calculated separately, and were then combined assuming statistical independence, which was shown to be a valid approximation using mock catalogues.

As described in the previous section, the calculation of the covariances related to the Spherical Harmonic modes requires a convolution of the galaxy power spectrum, allowing for the geometry of the survey and redshift-space distortions, and an additive shot noise term. In the absence of distortions, for an all-sky volume-limited survey with no noise, the modes are independent and their variance reduces to the power spectrum at the k -value corresponding to that Spherical Harmonic mode. This is analogous to analysis of all-sky noiseless CMB data (e.g. Bond et al. 2000; Verde et al. 2003), and results in a likelihood of the form

$$-2 \ln \mathcal{L} = \sum_{\text{modes}} \left[\ln P(k_i)^{\text{TH}} + \frac{\bar{\delta}^2(k_i)}{P(k_i)^{\text{TH}}} \right], \quad (2)$$

up to an irrelevant additive constant. Here $\bar{\delta}(k_i)$ gives the observed transformed overdensity field, and i indexes the Spherical Harmonics modes.

2.3 Choice of band-powers

In the analysis presented in this paper, the power spectrum was assumed to be constant within 16 bins in k -space covering the range of scales probed by the Spherical Harmonics analysis of P04. Although only Spherical Harmonic modes corresponding to $0.02 < k < 0.15 h \text{ Mpc}^{-1}$ were analysed, the geometry of the survey means that these modes have windows that extend beyond this range, and the power spectrum was therefore probed on both larger and smaller scales. However, the power spectrum is expected to become increasingly poorly constrained for $k < 0.02 h \text{ Mpc}^{-1}$ and $k > 0.15 h \text{ Mpc}^{-1}$ simply because modes with windows centred in these regions were excluded. The widths of the k -space bins used (given in Table 1) were chosen to reflect this.

Although each Spherical Harmonic mode has an associated window function, band-powers were fitted to the underlying unconvolved power spectrum. Because of this, the measured band-powers do not have windows: they do not cover an extended range in k . Model band-powers can therefore easily be calculated for a given cosmological model by averaging the model power spectrum across each bin. In addition to fitting the power spectrum shape through the band-powers, $\beta(L_*, 0)$ is also allowed to vary freely. The 17-dimensional likelihood space for these parameters has been mapped using the MCMC technique.

3 MCMC METHOD

The Markov Chain Monte Carlo (MCMC) method provides a mechanism to generate a random sequence of parameter values whose distribution matches the posterior probability distribution of a Bayesian analysis. This Section describes the method by which 4 chains, each containing > 60000 links, were produced mapping the 17-dimensional likelihood space consisting of the 16 band powers and $\beta(L_*, 0)$.

The 4 chains were started from widely separated points in parameter space and were constructed from this point using the Metropolis algorithm (Metropolis et al. 1953): given a chain at position \mathbf{x} , a candidate point \mathbf{x}' is chosen at random from a proposal

distribution $f(\mathbf{x}'|\mathbf{x})$. This point is always accepted, and the chain moves to point \mathbf{x}' , if the new position has a higher likelihood. If the new position \mathbf{x}' is less likely than \mathbf{x} , then \mathbf{x}' is accepted, and the chain moves to point \mathbf{x}' with probability given by the ratio of the likelihood of \mathbf{x}' and the likelihood of \mathbf{x} . In the limit of an infinite number of steps, the chains will reach a converged distribution where the distribution of chain links are representative of the likelihood hyper-surface, given any symmetric proposal distribution $f(\mathbf{x}'|\mathbf{x}) = f(\mathbf{x}|\mathbf{x}')$ (the Ergodic theorem: see, for example, Roberts 1996).

In the implementation of the MCMC method used in the 2dFGRS analysis presented in this paper, the proposal distribution was altered as the algorithm progressed in order to optimize the sampling of the likelihood surface. Dynamic optimization of the proposal function is a common feature of many MCMC analyses (see Gilks, Richardson & Spiegelhalter 1996 for examples). A multi-variate Gaussian proposal function was adopted, centered on the current chain position. The optimization of this proposal function requires an estimate of the covariance matrix for the likelihood surface at each step. Given such an estimate, the optimization proceeds as follows:

Along each principal direction corresponding to an eigenvector of the covariance matrix, the variance σ^2 of the multi-variate Gaussian proposal function was assumed to be a fixed multiple of the corresponding eigenvalue of the covariance matrix. The reasoning behind adopting this variation in the proposal width for different parameters is clear if the likelihood also has a multi-variate Gaussian form. Consider translating from the original 17 parameters to the set of parameters given by the decomposition along the principal directions of the covariance matrix each divided by the standard deviation in that direction. In this basis, the likelihood function is isotropic and the parameters are uncorrelated. Clearly an optimized proposal function will be the same in each direction, and we have adjusted the proposal function to have precisely this property. There is just a single parameter left to optimize – we are free to multiply the width of the proposal function by a constant in all directions. This overall normalization of the proposal width was dynamically adjusted to optimize chain convergence by giving a final acceptance rate, the proportion of candidate positions that are accepted, close to 0.25 (Gelman, Roberts & Gilks 1996). Note that the dynamic changing of the proposal function width violates the symmetry of the proposal distribution $f(\mathbf{x}'|\mathbf{x})$ assumed in the Metropolis algorithm. However, this was not a problem because we only used sections of the chains where variations between estimates of the covariance matrix were small.

Initially, a diagonal covariance matrix was assumed with a large variance for each of the 17 parameters, in order to quickly cover large regions of the 17-dimensional space. This estimate was then updated every 100 steps of the algorithm using the distribution of parameters within the last half of all 4 chains. The covariance matrix was found to rapidly converge to a stable solution. The dynamic covariance matrix calculation means that the step size decreases from a high initial value towards the value giving an average acceptance ratio of 0.25. The decreasing step-size reduces the burn-in time where the position of the chain is strongly dependent on the initial conditions. By considering the likelihood as a function of chain position, we adopt a very conservative value for the burn-in, and discard the first 10000 links from each chain. Convergence was confirmed using the method of Gelman & Rubin (1992), also described in Verde et al. (2003), although we have additionally tested that using only the first or second half of the 4 chains does not significantly affect the results of the analysis.

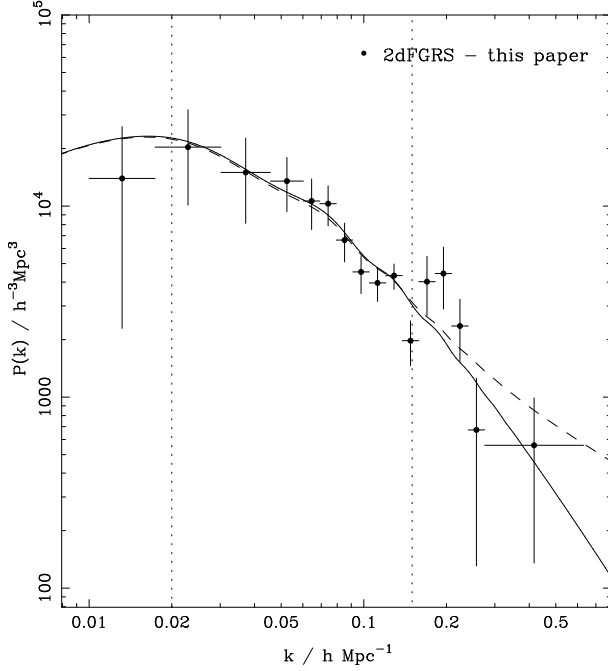


Figure 1. The real-space power spectrum of L_* galaxies calculated from the 2dFGRS (solid symbols). For comparison we also plot a model linear power spectrum with $\Omega_m h = 0.2$, $\Omega_b/\Omega_m = 0.15$, $b(L_*, 0)\sigma_8 = 0.8$, $n_s = 1.0$ and $h = 0.72$ (solid line). The dashed line shows that non-linear extrapolation of this model, calculated using the fitting formulae of Smith et al. (2003). Vertical dotted lines show the k -range chosen for the Spherical Harmonic modes fitted $0.02 < k < 0.15 h \text{ Mpc}^{-1}$.

Table 1. Marginalised real-space power spectrum band-powers calculated using the MCMC technique. Minimum and maximum $P(k)$ values correspond to $1\text{-}\sigma$ errors and were calculated using the form adopted for the likelihood (Eq. 4).

$k / h \text{ Mpc}^{-1}$		$P(k) / h^{-3} \text{ Mpc}^3$		
min	max	marg	min	max
0.0100	0.0174	13944.9	2289.3	26070.9
0.0174	0.0302	20343.2	10112.6	31912.1
0.0302	0.0457	14999.7	8118.1	22685.4
0.0457	0.0603	13505.5	9336.3	17958.2
0.0603	0.0692	10629.0	7528.0	13870.8
0.0692	0.0794	10296.7	7871.6	12776.1
0.0794	0.0912	6637.9	5106.3	8145.2
0.0912	0.1047	4521.1	3479.2	5503.3
0.1047	0.1202	3960.6	3167.7	4726.6
0.1202	0.1380	4326.7	3666.9	4971.0
0.1380	0.1585	1974.8	1460.5	2506.9
0.1585	0.1820	4019.1	2675.8	5461.1
0.1820	0.2089	4433.0	2889.0	6098.3
0.2089	0.2399	2357.5	1538.0	3251.3
0.2399	0.2754	673.6	130.6	1255.9
0.2754	0.6310	559.3	135.3	991.3

4 THE 2dFGRS REAL-SPACE POWER SPECTRUM

In Table 1 we present the recovered marginalised power spectrum band-powers calculated in 16 bins in k . These band-powers were calculated by averaging over the MCMC chains described in Section 3, discounting the burn-in period for each. The positions of the bins in k -space are also presented, as are approximate errors

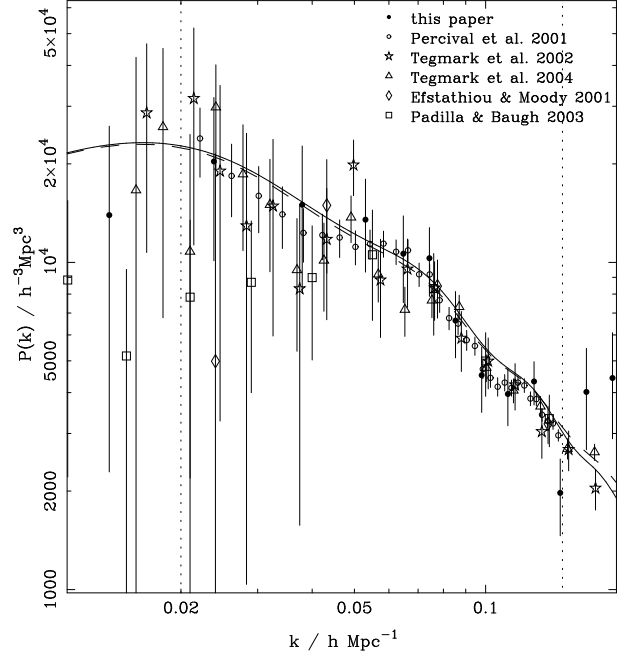


Figure 2. Comparison of large-scale galaxy power spectra shapes calculated from various galaxy surveys using different analysis methods. Although errors are plotted for each measurement, comparison of different errors is complicated by window functions and correlations between different data sets. The power spectra data that cover a range in k -space have been approximately corrected for their window functions by multiplying by the net effect of the window on a model power spectrum with $\Omega_m h = 0.165$, $\Omega_b/\Omega_m = 0.0$, $h = 0.72$ & $n_s = 1$. For clarity, the k -ranges covered by different data points are not shown in this figure. The amplitude of each power spectra has been matched to the measured real-space power spectrum of 2dFGRS L_* galaxies in this paper. The amplitude shifts required are given in Section 5, where details of the different data sets can also be found. The relative normalizations of the different power spectra are potentially due to a combination of galaxy bias, redshift-space and evolutionary effects depending on the sample. Note that a normalization correction is even required for SDSS L_* $P(k)$ data of Tegmark et al. (2004) as, due to red selection, the SDSS L_* galaxies are more biased than the 2dFGRS L_* galaxies.

for the points, calculated using the distribution described in section 6. In addition to these power spectrum measurements, we find that $\beta(L_*, 0) = 0.55$ with the $1\text{-}\sigma$ error region given by $0.46 < \beta(L_*, 0) < 0.64$, again given the distribution of $\beta(L_*, 0)$ values described in the next section.

The measured real-space power spectrum of L_* galaxies is plotted in Fig. 1. This plot shows that, as expected, although the band-powers extend beyond the k -range of modes selected for analysis ($0.02 < k < 0.15 h \text{ Mpc}^{-1}$) because of the window function caused by the survey geometry, they are only tightly constrained within this range. The real-space power spectrum is shown to be well matched to a standard concordance model ΛCDM power spectrum with $\Omega_m h = 0.2$, $\Omega_b/\Omega_m = 0.15$, $b(L_*, 0)\sigma_8 = 0.8$, $n_s = 1.0$ and $h = 0.72$.

5 COMPARISON WITH PREVIOUS GALAXY POWER SPECTRA

The shape of the measured 2dFGRS real-space power spectrum of L_* galaxies (solid circles) is compared with other measure-

ments of galaxy power spectra in Fig. 2. Because of correlations between different data points in the same power spectrum and window functions associated with some measurements, it is difficult to compare error bars and the relative constraints on cosmological models placed by different data sets. The easiest way to compare the significance of the different data sets is to consider parameter constraints for the same k -range and cosmological model. This is not attempted in this paper. Instead, Fig. 2 is included simply to demonstrate the incredible consistency in the large-scale ($0.02 < k < 0.15 h \text{ Mpc}^{-1}$) shape of recent measurements of galaxy power spectra.

In Fig. 2 we plot two estimates of the 2dFGRS power spectrum shape in addition to the present analysis. The redshift-space data of Percival et al. (2001) are plotted as open circles. These data were calculated from the 160000 galaxy redshift measured before February 2001, and $P(k)$ was multiplied by 0.69 to match the present data. This factor is expected to be due to a combination of redshift-space effects and luminosity-dependent bias (the Percival et al. 2001 data are not corrected to correspond to L_* galaxies). We also plot the measurement of the 2dFGRS power spectrum from the first 100000 galaxies of measured by Tegmark, Hamilton & Xu (2002) – open stars. These $P(k)$ data required multiplication by a factor 0.61 to match the amplitude of the real-space power spectrum measured in this work. The Tegmark et al. (2002) analysis method was strongly affected by luminosity-dependent bias, potentially leading to a tilt in the recovered power spectrum, and a different overall amplitude (Percival, Verde & Peacock 2003).

We also plot the SDSS power spectrum of Tegmark et al. (2004) as open triangles in Fig. 2. The data of Tegmark et al. (2004) are crudely corrected for bias by dividing by an effective (bias)² at each k -value. While this corrects for an overall normalization offset, there is an additional minor effect caused by the change in survey geometry that is not corrected in this approach (Percival, Verde & Peacock 2003). In the Spherical Harmonics analysis of the 2dFGRS data presented here, the data are corrected for variable bias in a self-consistent way. The SDSS data of Tegmark et al. (2004) required a downward correction by a factor 0.77 to match the normalization of the 2dFGRS data, presumably because of a difference in the bias of 2dFGRS L_* and SDSS L_* galaxies.

We have also compared our power spectrum to that recovered by deprojecting the APM survey, the parent survey to the 2dFGRS. Results from analyses of Efstathiou & Moody (2001) – open diamonds, and Padilla & Baugh (2003) – open squares, are plotted and shown to be in satisfactory agreement. There is weak evidence that these power spectra have less power on large scales ($k \sim 0.03$) than the data from the redshift surveys, but given the large errors on the deprojected power spectra, this deviation is not significant. The offsets required for these data sets to match the 2dFGRS $P(k)$ normalization were 0.79 and 0.62 for the data of Efstathiou & Moody (2001) and Padilla & Baugh (2003) respectively.

6 FITTING TO THE LIKELIHOOD DISTRIBUTION

In this Section we use the MCMC chains described in Section 3 to determine a simple model of the likelihood surface. If, to the accuracy of the present power spectrum constraints, there is little data loss compressing the model power spectrum into the 16 band-powers described in Section 2.3, then this will provide a method for quickly estimating the likelihood of a cosmological model.

The basic problem is to find an accurate description of the 17-parameter likelihood hyper-surface. From Eq. 2 it is immediately

clear that, even for an all-sky volume-limited noiseless survey of a clustered field, the true likelihood is not symmetric in $P^{\text{TH}}(k_i)$ about any point. This rules out a Gaussian likelihood distribution of the form

$$-2 \ln \mathcal{L} \propto \sum_{ij} [Q_i^{\text{TH}} - Q_i] M_{ij} [Q_j^{\text{TH}} - Q_j], \quad (3)$$

with $Q_i = P(k_i)$ for $1 < i < 16$, $Q_{17} = \beta(L_*, 0)$ and fixed inverse covariance matrix M_{ij} . Assuming such a distribution would result in a biased estimate of the likelihood surface.

This could be corrected either by allowing the inverse covariance matrix to be a function of the model being tested or by considering a different form for the likelihood, for example by allowing $Q_i = f_i[P(k_i)]$, $1 < i < 16$ and $Q_{17} = f_{17}[\beta(L_*, 0)]$ to be more general functions of the band powers and $\beta(L_*, 0)$. In this case, M_{ij} would be assumed to be independent of the model to be tested.

This problem is analogous to the compression of CMB maps into a series of band-powers and has been considered in that context by a number of authors. In particular, Bond et al. (2000) suggest assuming an offset lognormal likelihood distribution for CMB band powers. For the real-space band powers and $\beta(L_*, 0)$ this corresponds to assuming that the likelihood is given by Eq. 3, but with $Q_i = \ln[P(k_i)] \bar{P}_i$, $1 < i < 16$ where \bar{P}_i is the maximum likelihood band-power, and similarly for $\beta(L_*, 0)$. Bond et al. (2000) argued that this change of variables retains the true curvature matrix calculated from Eq. 1 in the case of an all-sky CMB map with no noise (i.e. the correct behaviour of the likelihood around the peak). In addition, for an all-sky CMB map with no noise, the offset lognormal distribution is approximately skewed beyond the peak in the expected fashion given the dependence on the theoretical power displayed by the true likelihood. This argument also applies to the galaxy distribution being analysed in this paper.

Although both of the Gaussian and offset log-normal distributions provide the correct curvature around the peak of the likelihood, it is not clear that either provides an unbiased likelihood surface beyond this point, particular when noise and correlations become important. In a recent analysis of the WMAP CMB data, Verde et al. (2003) considered a combination of Gaussian and log-normal likelihoods, which automatically matches the peak curvature, but additionally matches the behaviour around the peak for the case of an all-sky CMB map with no noise. In order to do this, a likelihood distribution of the form $\ln \mathcal{L} = 1/3 \ln \mathcal{L}_{\text{Gauss}} + 2/3 \ln \mathcal{L}_{\text{OLN}}$ was adopted, where $\mathcal{L}_{\text{Gauss}}$ and \mathcal{L}_{OLN} are the Gaussian and offset lognormal likelihoods respectively.

However, for the Spherical Harmonics analysis considered here, both shot noise and coupling between modes are significant, and the behaviour around the likelihood peak is not so easily estimated analytically. The good news is that the MCMC technique produces a sampling of the likelihood surface that can be fitted. Given a chain of values that sample the hyper-surface, estimating the likelihood distribution for a given parameter, marginalising over the other 16 parameters simply involves binning all of the values in the chain. For the band-powers and $\beta(L_*, 0)$ the marginalised distributions were found to be well fitted by Gaussian distributions in

$$Q_i = a_i P_i + (1 - a_i) \ln[P_i] \bar{P}_i, \quad (4)$$

the form of which was motivated by the Gaussian and offset log-normal distributions discussed above. Here, we define $P_i \equiv P(k_i)$ for $1 < i < 16$ and $P_{17} \equiv \beta(L_*, 0)$ and similarly for the maximum likelihood positions \bar{P}_i . The best fit values of \bar{P}_i and a_i (with the constraint $0 < a_i < 1$) were fitted for each band-

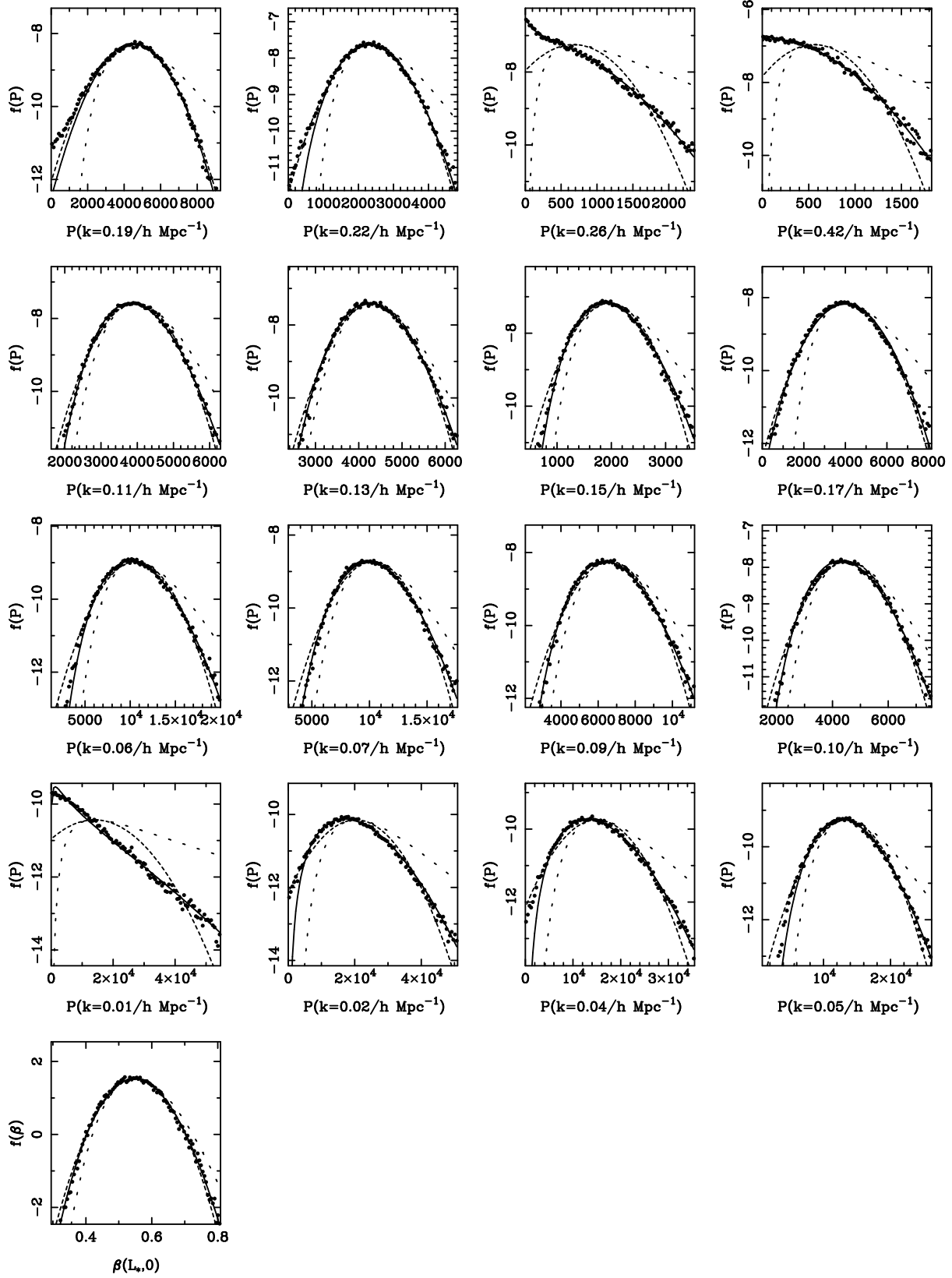


Figure 3. The distribution of the 16 recovered band-power values and $\beta(L_*, 0)$, calculated from the MCMC chains. Each distribution has been calculated after marginalising over the remaining 16 parameters (solid symbols). This distribution has been fitted with a Gaussian (dashed line), and a log-normal distribution with maximum at the distribution mean (dotted line). We have also fitted the distribution assuming that the distribution is Gaussian, not in the band-power (or $\beta(L_*, 0)$), but in a linear combination of the band-power and its logarithm (solid line).

Table 2. Parameters of the likelihood surface fits given by Eqns. 3 & 4. For each band-power these data were calculated by fitting the MCMC output marginalised over the remaining 16 parameters, as described in Section 6. In addition $a = 0.689$ and $\bar{\beta}(L_*, 0) = 0.551$ were obtained from the fit to the marginalised likelihood as a function of $\beta(L_*, 0)$.

$k / h \text{ Mpc}^{-1}$		a	$\bar{P}(k) / h^{-3} \text{ Mpc}^3$
min	max		
0.0100	0.0174	0.243	9192.4
0.0174	0.0302	0.543	19588.3
0.0302	0.0457	0.542	14547.5
0.0457	0.0603	0.544	13326.2
0.0603	0.0692	0.539	10476.3
0.0692	0.0794	0.564	10194.9
0.0794	0.0912	0.483	6534.5
0.0912	0.1047	0.465	4429.4
0.1047	0.1202	0.486	3907.2
0.1202	0.1380	0.473	4292.9
0.1380	0.1585	0.503	1948.7
0.1585	0.1820	0.914	4046.9
0.1820	0.2089	1.000	4493.6
0.2089	0.2399	0.770	2357.5
0.2399	0.2754	0.514	542.9
0.2754	0.6310	0.557	470.0

power and $\beta(L_*, 0)$ to the distribution of parameter values in the chains, and are given in Table 2. Note that the maximum likelihood band-powers $\bar{P}(k_i)$ differ from the marginalised band-powers given in Table 1 as expected if the distributions are not symmetric. Plots showing the fits are presented in Fig. 3. Outside of the range of nodes probed in P04 ($0.02 < k < 0.15 h \text{ Mpc}^{-1}$) the probability distribution of band-powers is strongly non-Gaussian. However, assuming Gaussianity in Q_i (Eq. 4) rather than the band-powers provides a reasonable fit to the recovered distribution. The covariance matrix was found from the MCMC chains assuming Gaussianity in Q_i (i.e. from the expected multiples $\langle Q_i Q_j \rangle$), and was inverted to give M_{ij} . The best-fit values of \bar{P}_i , a_i and the corresponding inverse covariance matrix M_{ij} are available from <http://www.roe.ac.uk/~wjrp/>.

7 TESTING THE LIKELIHOOD SURFACE

The 4-parameter set of cosmological models considered by P04 has been used to compare the estimated likelihoods with those calculated directly from the Spherical Harmonics procedure, where for each model a covariance matrix is constructed and used to calculate the likelihood through Eq. 1. In this set of models, the matter density multiplied by the Hubble constant $\Omega_m h$, baryon fraction Ω_b / Ω_m , power spectrum normalization $b(L_*, 0) \sigma_8$ and $\beta(L_*, 0)$ were allowed to vary, while scalar spectral index $n_s = 1.0$ & Hubble constant $h = 0.72$ were fixed. Model band-powers were calculated by averaging the Eisenstein & Hu (1998) power spectrum fits over each bin in $\log(k)$. The power spectra were extrapolated into the non-linear regime using the fitting formulae of Smith et al. (2003).

Fig. 4 compares the 1d marginalised likelihoods from the two methods of likelihood calculation. Good agreement is demonstrated between the true and estimated likelihood surfaces. There is weak evidence for a slight bias to slightly higher $b(L_*, 0) \sigma_8$ and lower $\beta(L_*, 0)$ values. In Fig. 5 we show contour plots of the marginalised likelihood for each 2-parameter combination (our 4

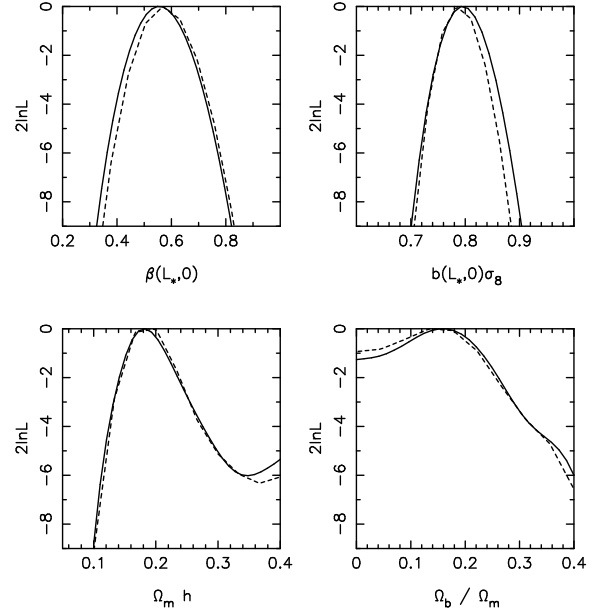


Figure 4. Marginalised likelihoods for the 4 parameter Λ CDM cosmological model considered by P04 with $h = 0.72$ and $n_s = 1.0$. The dashed line was calculated directly from the Spherical Harmonics procedure – for each model, a covariance matrix is constructed and applied to calculate the likelihood. The solid lines were calculated assuming that the 16 $P(k)$ measurements and $\beta(L_*, 0)$ have a Gaussian distribution in the functions given by Eq. 4.

parameter model has 6 distinct pairs of parameters). This shows that $b(L_*, 0) \sigma_8$ and $\beta(L_*, 0)$ are anti-correlated and the offsets in $b(L_*, 0) \sigma_8$ and $\beta(L_*, 0)$ are therefore related. The difference could be caused by inaccuracies in the likelihood model fits of Eq. 4, or due to information loss because of the data compression into 17 parameters. However, the offset is significantly smaller than any errors that would be placed on either parameter from this analysis, and is not therefore of major concern.

8 SUMMARY & DISCUSSION

A new method using the MCMC technique has been developed to recover the real-space power spectrum from a decomposition of a galaxy overdensity field and has been applied to the 2dFGRS Spherical Harmonics analysis presented in P04. The recovered 2dFGRS L_* power spectrum was presented as 16 marginalised power spectrum band-powers. The MCMC technique was also used to obtain information about the shape of the likelihood surface. Using this information, the likelihood surface was fitted with a simple model, providing a quick method for estimating the likelihood of different cosmological models.

The advantage of the MCMC method over previous deconvolution routines lies in providing a map of the likelihood surface. Maximum likelihood techniques have previously been used to recover the real-space power spectrum in a series of band-powers (Ballinger, Heavens & Taylor 1995), using a standard routine to iterate to the likelihood maxima. However, such a step-wise maximum likelihood method only partially explores the likelihood surface giving poorly determined conditional errors (Ballinger et al. 1995; Tadros et al. 1999). The MCMC technique provides a significant advance over such methods, as it enables a more complete exploration of the likelihood surface to be quickly undertaken.

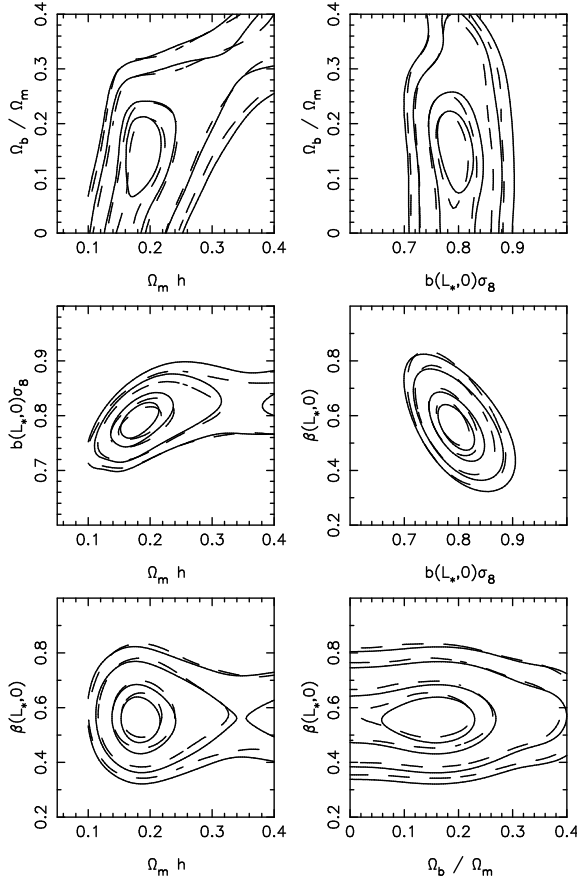


Figure 5. Contour plots showing changes in the likelihood from the maximum of $2\Delta \ln \mathcal{L} = 1.0, 2.3, 6.0, 9.2$ for different parameter combinations for the combined likelihood from the 2dFGRS NGP and SGP catalogues, assuming a Λ CDM power spectrum with $h = 0.72$ and $n_s = 1.0$. Dashed contours were calculated directly from the Spherical Harmonics procedure and correspond to those in fig. 6 in P04. Solid contours were calculated assuming that the 16 $P(k)$ measurements and $\beta(L_*, 0)$ have a Gaussian distribution in the functions given by Eq. 4. Solid and dashed lines therefore correspond to the 1D marginalised likelihood curves presented in Fig. 4.

An alternative to the step-wise approach to determining ML band-powers, is to use quadratic band-power estimators (Hamilton 1997a;b) favoured by Tegmark et al. (2002; 2004). The band-powers that we model have no window functions, and therefore must correspond to the linear combinations of the quadratic estimators given by the inverse of the Fisher information matrix (see, for example, section 3.5 of Tegmark et al. 2002). In this approach, the resulting band-powers are assumed to have a Gaussian likelihood with model-independent covariances, which, as we argued in Section 2.2, for an all-sky noiseless survey must lead to a different form for the likelihood compared with the true likelihood given by Eq. 2. This is consistent with the MCMC analysis presented in this paper which suggests that the likelihood distribution around the band-powers is not well described by a multi-variate Gaussian distribution. Either the covariance matrix must change its form, or equivalently the shape of the function assumed for the likelihood surface must change. The MCMC technique is therefore advantageous over the quadratic band-power method as it provides the information required to allow the likelihood surface to be accurately modelled beyond the likelihood peak.

Another factor that makes the MCMC routine particularly well

suited to this application is the nature of the likelihood surface. No evidence was found for multiple likelihood maxima, which would slow the MCMC mapping. Additionally, more simple techniques would fail because the surface does not follow an obvious form – for instance it is close to, but not exactly a multi-variate Gaussian so a simple fit of a multi-variate Gaussian would be inappropriate. Fitting to the likelihood surface has been shown to provide an accurate estimate of the combined likelihoods for a number of cosmological models covering a range of power spectrum shapes. This gives us confidence that it can be extended to cover a wider range of cosmological models.

From the MCMC chains, we have estimated marginalised band-powers, and have compared these with measurements of the real-space power spectrum from the SDSS, and with other measurements from the 2dFGRS. Excellent agreement is observed and the basic shape of the power spectrum now seems to be well constrained. We have not directly compared with the real-space power spectrum of the IRAS 1.2Jy galaxies (Ballinger et al. 1995) or with the real-space power spectrum of the PSCz galaxies estimated by Tadros et al. (1999), in order not to further clutter Fig. 2. However, it is worth noting that the general shape of the recovered power spectra are similar. We have compared with the deprojected APM data of Efstathiou & Moody (2001) and Padilla & Baugh (2003), although the 2dFGRS and SDSS data represent a significant improvement over these data.

In addition to the band-power measurements we simultaneously fit the linear redshift-space distortions. A best-fit value of $\beta(L_*, 0) = 0.55$ was recovered with $1-\sigma$ confidence region given by $0.46 < \beta(L_*, 0) < 0.64$. This compares very well with the value of $\beta(L_*, 0) = 0.58 \pm 0.08$ recovered in P04 marginalising over the basic set of cosmological models considered. Note that from the approximation to the likelihood we recover the same parameter value if we consider the range of models chosen, and their associated priors on the shape of the power spectrum.

The marginalised band-power and $\beta(L_*, 0)$ measurements were presented in Table 1. These should not be confused with the parameters of the fit to the likelihood surface that were presented in Table 2 and associated covariance matrix. All of these data are publicly available from <http://www.roe.ac.uk/~wjp/>, where simple segments of code demonstrating how the likelihood can be quickly calculated are also provided. It should therefore be possible to easily combine the cosmological constraints provided by the Spherical Harmonics analysis of P04 with other cosmological probes.

Obviously, these constraints should not be combined with other analyses of the 2dFGRS such as provided by Percival et al. (2001) or Cole et al. (2004) as these results are strongly inter-dependent. The analysis presented by Cole et al. (2004) uses more galaxies and therefore provides tighter constraints on the power spectrum shape than the Spherical Harmonics analysis considered here and should be used in preference to this work if the power spectrum shape is the important consideration. The advantage of the Spherical Harmonics analysis is that, although it provides weaker information on $P(k)$ shape, it provides additional correlated information about $\Omega_m^{0.6}\sigma_8$ from fitting the redshift-space distortions.

An example application where using Spherical Harmonics rather than Fourier likelihoods may be advantageous is to provide constraints on the neutrino mass density. Here, the amplitude of the low-redshift matter power spectrum provides a significant constraint, and has previously been determined by converting a redshift-space power spectrum amplitude to σ_8 using β and galaxy

bias b calculated from other analyses (e.g. Spergel et al. 2003). The problem with such an approach is that β and b are often measured on different scales, using different analysis techniques and model dependencies. The Spherical Harmonics method instead sets a constraint on σ_8 (through $\Omega_m^{0.6} \sigma_8$) in a self-consistent way. Combining the Spherical Harmonics likelihoods with CMB likelihoods should therefore provide a more robust determination of the neutrino mass density.

ACKNOWLEDGMENTS

The author wishes to thank the staff of the Anglo-Australian Observatory and the 2dFGRS team members whose dedicated work provided this wonderful survey data. Useful discussions with Alan Heavens and John Peacock concerning likelihood calculation and the Spherical Harmonics method were also of great help. The anonymous referee's comments led to a significant improvement in the presentation of this work. WJP is supported by PPARC through a Postdoctoral Fellowship.

REFERENCES

- Ballinger W.E., Heavens A.F., Taylor A.N., 1995, MNRAS, 276, L59
 Bond J.R., Jaffe A.H., Knox L., 2000, ApJ, 533, 19
 Cole S., et al., 2004, in preparation
 Colless M., et al., 2003, astro-ph/0306581
 Efsthathiou G., Moody S.J., 2001, MNRAS, 325, 1603
 Eisenstein D.J., Hu W., 1998, ApJ, 496, 605
 Feldman H.A., Kaiser N., Peacock J.A., 1994, ApJ, 426, 23
 Fisher K.B., Scharf C.A., Lahav O., 1994, MNRAS, 266, 219
 Fisher K.B., Lahav O., Hoffman Y., Lynden-Bell D., Zaroubi S., 1995, MNRAS, 272, 885
 Gelman A., Rubin D., 1992, *Statistical Science* 7, 457
 Gelman A., Roberts G.O., Gilks W.R., 1996, in eds Bernardo J.M., Berger J.O., Dawid A., Smith A., *Bayesian Statistics 5*, 599, OUP
 Gilks W.R., Richardson S., Spiegelhalter D.J., *Markov chain monte carlo in practice*, 1996, Chapman & Hall
 Hamilton A.J.S., 1997a, MNRAS, 289, 285
 Hamilton A.J.S., 1997b, MNRAS, 289, 295
 Hamilton A.J.S., Tegmark M., Padmanabhan N., 2000, MNRAS, 317, L23
 Heavens A.F., Taylor A.N., 1995, MNRAS, 275, 483
 Kaiser N., 1987, MNRAS, 227, 1
 Metropolis N., Rosenbluth A.W., Rosenbluth M.N., Teller A.H., Teller E., 1953, *Journal of Chemical Physics*, 21, 1087
 Norberg P., et al. (The 2dFGRS Team), 2001, MNRAS, 328, 64
 Padilla N.D., Baugh C.M., 2003, MNRAS, 343, 796
 Percival W.J., et al., 2001, MNRAS, 327, 1297
 Percival W.J., Verde L., Peacock J.A., 2004, 347, 645
 Percival W.J., et al., 2004, P04, MNRAS accepted, astro-ph/0406513
 Pope A.C., et al., 2004, ApJ, 607, 655
 Roberts G.O., 1996, in eds Gilks W.R., Richardson S., Spiegelhalter D.J., *Markov chain monte carlo in practice*, Chapman & Hall
 Smith R.E., et al., 2003, MNRAS, 341, 1311
 Spergel D.N., et al., 2003, ApJS, 148, 175
 Tadros H., et al., 1999, MNRAS, 305, 527
 Tegmark M., Hamilton A.J.S., Xu Y., 2002, MNRAS, 335, 887
 Tegmark M., et al., 2004, ApJ, 606, 702
 Verde L., et al., 2003, ApJS, 148, 195